

**Electronic Supplementary Information**

**Precursors for PbTe, PbSe, SnTe, and SnSe Synthesized Using  
Diphenyl Dichalcogenides**

Zhongyong Wang,<sup>a</sup> Yuanyu Ma,<sup>a</sup> Prathamesh B. Vartak,<sup>a</sup> and Robert Y. Wang<sup>a\*</sup>

<sup>a</sup>*School for Engineering of Matter, Transport & Energy, Arizona State University, Tempe, Arizona  
85287*

*E-mail: rywang@asu.edu*

**Experimental Methods**

**Chemicals and Materials**

Diphenyl diselenide (180629, 98%) and diphenyl ditelluride (384127, 98%) were acquired from Sigma Aldrich. Lead powder (00942, 99%) and Tin powder (11013, 99.995%) were purchased from Alfa Aesar. Ethylenediamine (03550, >99.5%) and pyridine (270970, 99.8%) were purchased from Sigma Aldrich. Butylamine (L03575, 99%) and dimethyl sulfoxide (276855, >99.9%) were purchased from Alfa Aesar and Sigma Aldrich, respectively. Sodium Sulfide (99.9%) was purchased from Advanced Chemicals.

**Precursor Synthesis and Characterization**

Unless otherwise indicated, all precursor synthesis, processing, and decomposition was carried out in a nitrogen-filled glovebox. SnSe, SnTe, PbSe, PbTe and PbSe<sub>x</sub>Te<sub>1-x</sub> precursors were prepared by mixing metal powder and diphenyl dichalcogenide in a variety of solvents. For PbSe precursor preparation, 0.32 mmol tin and 0.32 mmol diphenyl diselenide was dissolved in 1 mL ethylene diamine (EDA), dimethyl sulfoxide, butylamine, or pyridine, respectively. The mixture was then stirred for 24 h and filtered using a PVDF filter with a pore size of 2 μm. SnTe, SnSe and PbTe precursors were prepared in an analogous manner. To prepare PbSe<sub>x</sub>Te<sub>1-x</sub> alloy precursors, 0.32 mmol lead was mixed and 0.32 mmol of diphenyl dichalcogenide (with an appropriate ratio of diphenyl diselenide to diphenyl ditelluride) was dissolved in 1 mL EDA. The as-synthesized SnSe, SnTe, PbSe, PbTe and PbSe<sub>x</sub>Te<sub>1-x</sub> precursors were characterized using a thermogravimetric analyzer (Labsys Evo). Thermogravimetric analysis (TGA) sample was prepared by drop-casting the precursor solution to a pre-cleaned silicon substrate and drying at room temperature for 48 h in a nitrogen-filled glovebox. The solidified precursor was scratched off the substrate and sealed in a vial inside the glovebox for transfer to the TGA. During TGA, the sample was heated from room temperature to 500 °C at a heating rate of 2 °C min<sup>-1</sup> in a helium atmosphere. It took ~5-10 minutes to transfer the vial from the glovebox to the TGA, and so a brief and limited oxygen exposure occurred at that time. Powder x-ray diffraction (XRD) was used to determine the crystal structure of samples after thermal decomposition. XRD samples were prepared by drop-casting precursor solution onto the silicon substrate and heating it at 400 °C

for 120 minutes. High-resolution XRD was performed using a PANalytical X'Pert PRO MRD with Cu K $\alpha$  X-ray source operating at 40 kV and 40 mA.

### **PbSe<sub>x</sub>Te<sub>1-x</sub> Thin Film Deposition and Characterization**

For PbSe<sub>x</sub>Te<sub>1-x</sub> thin film preparation, PbSe<sub>x</sub>Te<sub>1-x</sub> precursors were spin-coated onto either silicon or quartz substrates with a speed of 1800 RPM for 30 s. Then the sample was annealed at 250 °C for 30 min and further annealed at 400 °C for another 30 min. For Na-doped PbSe<sub>x</sub>Te<sub>1-x</sub> thin film preparation, 25.9 mg Na<sub>2</sub>S was added to 1 mL EDA and stirred overnight. Note that Na<sub>2</sub>S has poor solubility in EDA and so a large quantity of Na<sub>2</sub>S (e.g. more than half) didn't dissolve. This mixture was then filtrated using a PVDF filter and subsequently diluted by a factor of 10 with EDA. 5  $\mu$ L of this diluted Na<sub>2</sub>S solution was added to 200  $\mu$ L of the PbSe<sub>x</sub>Te<sub>1-x</sub> precursor solution and then filtered again using a PVDF filter. We then spin-coated this solution onto quartz substrates with a speed of 1800 RPM for 30 s. The film was then annealed at 250 °C for 30 min and further annealed at 400 °C for another 30 min. We designate these Na-doped samples in the paper as “moderately Na-doped.”

We prepared “lightly Na-doped” samples by taking the abovementioned dilute Na<sub>2</sub>S solution in EDA and further diluting it by a factor of 10. 5  $\mu$ L of this more dilute solution was added to 200  $\mu$ L of PbSe<sub>x</sub>Te<sub>1-x</sub> precursor solution to prepare “lightly Na-doped” PbSe<sub>x</sub>Te<sub>1-x</sub> thin films.

The microstructure of the PbSe<sub>x</sub>Te<sub>1-x</sub> thin films was characterized using a FEI XL-30 scanning electron microscope (SEM). Film thickness was determined by scratching the film and then conducting profilometry using a Bruker Dektak XT profilometer. The typical scratch profile is shown in Figure S2 for undoped, lightly-doped and moderately-doped PbSe<sub>x</sub>Te<sub>1-x</sub> thin films. Table 1 lists the film thicknesses of these samples. Rutherford backscattering spectroscopy (RBS) was done using a 1.7 MV Tandatron Ion Accelerator made by General Ionex. The RBS data was collected using 3 MeV He<sup>2+</sup> ions and analyzed using SIMRNA. X-ray photoelectron spectroscopy (XPS) measurements were carried out in a VG 220i-XL instrument with a monochromated Al K-alpha X-ray as the source. The analysis was done in an ultra-high vacuum system (10<sup>-9</sup> Torr). Dynamic secondary ion mass spectroscopy (SIMS) was carried out using a Cameca IMS 6F. The analysis was carried out using O<sub>2</sub><sup>++</sup> primary-ion bombardment (12.5 kV, 25 nA) and positive secondary-ion detection. The raster size is 250  $\mu$ m and the analyzed area is 60  $\mu$ m across. Ion beam sputtering time was converted into penetration depth with profilometry measurements.

### **Thermoelectric Property Measurement**

Electrical conductivity measurements were performed using the van der Pauw method and conducted on the same samples used to measure the Seebeck coefficient. Samples for electrical conductivity and Seebeck coefficient measurements were prepared on quartz substrates. The use of electrically insulating quartz substrates ensures that all charge transport occurs within the thin film sample itself (i.e. as opposed to the substrate). Seebeck coefficient and electrical conductivity measurements were also done in a nitrogen-filled glovebox to ensure that the samples were not affected by oxidation.

The electrical sheet resistance was measured using a Keithley 2400 Source meter by taking current-voltage data at 10 points for currents ranging from -50 to +50  $\mu\text{A}$ . The sample thickness was measured by scratching the sample and performing profilometry at the scratch location. The sheet resistance was then divided by the sample thickness to get electrical conductivity.

Seebeck coefficient measurements were performed using the steady-state slope method. The temperature gradient for the Seebeck coefficient measurement was created using two commercially available thermoelectric devices to heat and cool opposite ends of the sample. The heating and cooling of the sample was applied such that the average sample temperature was approximately room temperature. The temperatures at the hot and cold ends of the sample were measured using T-type thermocouples and a Stanford Research Systems SR630 Thermocouple Reader. A small amount of thermal paste was used to minimize the thermal contact resistance between the thermocouples and the samples. In addition, thin gauge thermocouples (40 AWG gage) were used to minimize cold finger effects from the thermocouple wire.<sup>1</sup> The open circuit voltage was measured for six temperature differences ranging from -20 to +20  $^{\circ}\text{C}$  using an Agilent 34401A Multimeter. Plotting a curve of voltage ( $V$ ) versus temperature difference ( $\Delta T$ ) and then taking the negative slope of the curve yields the Seebeck coefficient,  $S = -V/\Delta T$ . A positive Seebeck coefficient indicates that the sample is p-type and that the cold region of the sample develops a higher potential than the hot region. The temperature uncertainties in the sample's hot and cold regions were the dominant contributor to the uncertainty in each Seebeck coefficient measurement. This resulted in a Seebeck coefficient measurement uncertainty of  $\pm 10\%$ .

## Results

### RBS Analysis

RBS spectra raw data is shown in Fig. S3. The  $\text{He}^{2+}$  ions that backscattered from collisions with Pb, Te and Se atoms in the film are shown at approximate channel numbers 630, 680 and 713, which correspond to the backscattered ion energy of 3436, 3715 and 3896 eV, respectively. SIMRNA was used for doing simulation for RBS analysis to obtain the Se/Te ratio.

### XPS Analysis:

X-ray photoelectron spectroscopy measurements (Fig. S4) reveal the elemental electronic states and the elemental composition near the film surface. Figure 4a shows the survey spectrum for  $\text{PbSe}_{0.56}\text{Te}_{0.44}$  thin films spanning 100 – 600 eV. Fig. S4b, S4c and S4d are the high energy-resolution spectra for Pb 4f, Se 3d and Te 3d regions, respectively.

The Se/Te atomic ratio in the thin film surface can be extracted from the survey spectrum (Figure S4a), which is summarized in Table S2. These results matched well with the RBS results, which suggests a uniform elemental distribution of Se and Te from film surface to film interior.

### **SIMS Analysis**

The raw data for our SIMS analysis is shown in Figure S5. The SIMS signals depends on the element concentration and element's ionization properties. In order to assess the Na concentration in our samples, we assumed that the Pb concentration was equivalent in all samples. This then allows us to assess the relative concentration of Na across all three doping levels. We note that a numeric quantification of Na concentration using SIMS would require an equivalent  $\text{PbSe}_{0.56}\text{Te}_{0.44}$  thin film sample with known Na concentration as a reference sample, which was not possible to create in this work.

### **Thermoelectric Property Analysis**

The positive value of the Seebeck coefficient indicates that our  $\text{PbSe}_{0.56}\text{Te}_{0.44}$  films are p-type. The increase in Seebeck coefficient and decrease in electrical conductivity as Na-doping increases suggests that Na-doping is decreasing the hole concentration (i.e. that Na-doping is moving the Fermi level away from the valence band edge). We note that Na is typically a p-type dopant in lead chalcogenides,<sup>2</sup> and so one would typically expect Na to increase the hole concentration. While this differs from our observation, one possibility that could explain our results is to consider the lattice sites of the Na dopants. Deposition of metal chalcogenide semiconductors from precursors (e.g. hydrazine-based and diamine/dithiol-based precursors) commonly result in stoichiometries that are slightly metal-deficient (chalcogen-rich). This suggests that our  $\text{PbSe}_{0.56}\text{Te}_{0.44}$  films contain Pb-vacancies, which can potentially donate two holes per Pb-vacancy. This is consistent with our observed p-type transport in our undoped films (i.e. positive Seebeck coefficient). While Na typically functions as a p-type dopant<sup>3</sup> by substituting into Pb-sites, we suspect a significant fraction of our Na dopants are instead occupying Pb-vacancy-sites. In this scenario, the overall hole concentration in our samples would decrease because a Na-occupied Pb-site can only yield one hole whereas a Pb-site-vacancy can potentially yield two holes (see Scheme S1). It is important to note that this explanation for our observed Na-doping effects is only a hypothesis at this time and that more studies are needed.

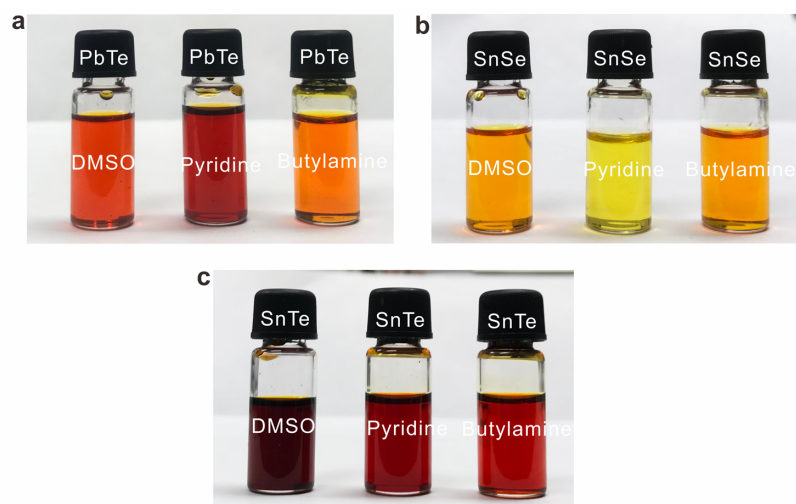


**Figure S1.** Photographs of as-synthesized (a) PbTe, (b) SnSe, and (c) SnTe precursors prepared in dimethyl sulfoxide (DMSO), pyridine and butylamine, respectively, as shown from left to right.

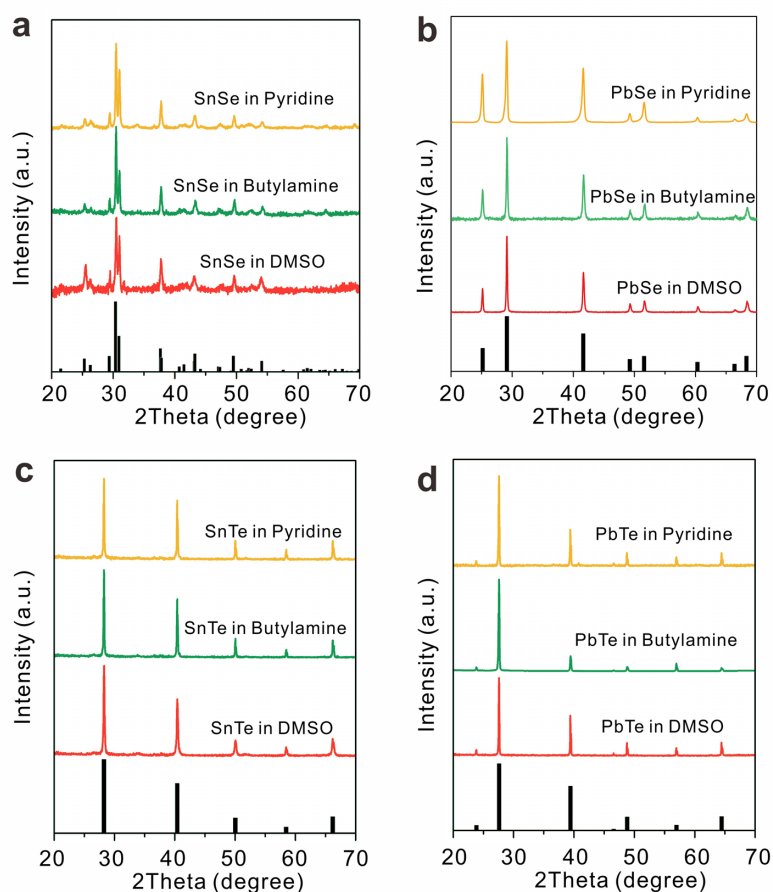


**Figure S2.** X-ray diffraction patterns of products recovered from (a) SnSe, (b) PbSe, (c) SnTe, and (d) PbTe precursors prepared in pyridine, butylamine, and dimethyl sulfoxide (DMSO), after annealing at 400 °C for 2 h in a nitrogen-filled glovebox.

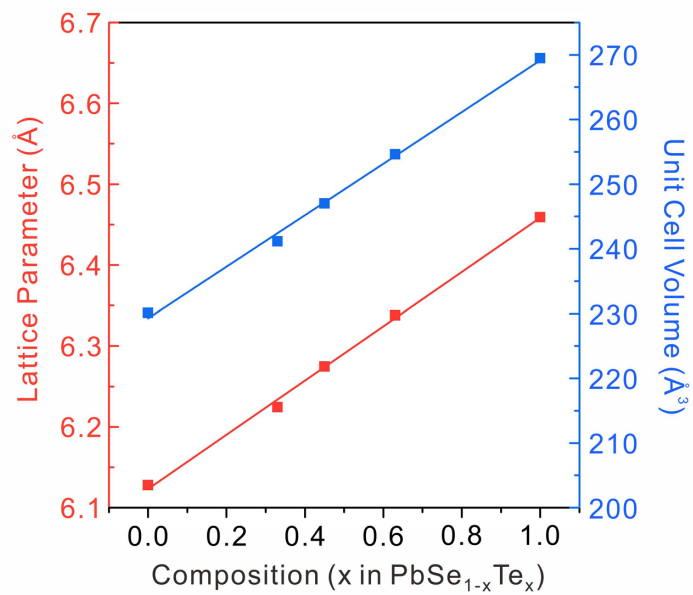


**Figure S3.** Linear relationships between the lattice parameter and unit cell volume as a function of experimentally determined composition of PbSe<sub>1-x</sub>Te<sub>x</sub>.

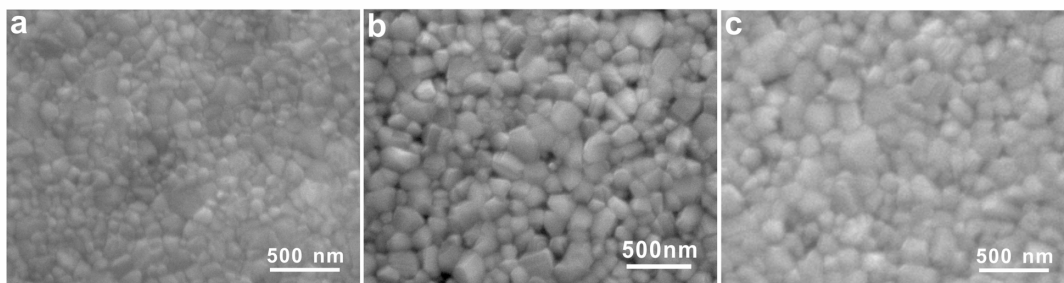


**Figure S4.** SEM image of PbSe<sub>0.67</sub>Te<sub>0.33</sub> (a), PbSe<sub>0.55</sub>Te<sub>0.45</sub> (b), and PbSe<sub>0.37</sub>Te<sub>0.63</sub> (c) thin films.

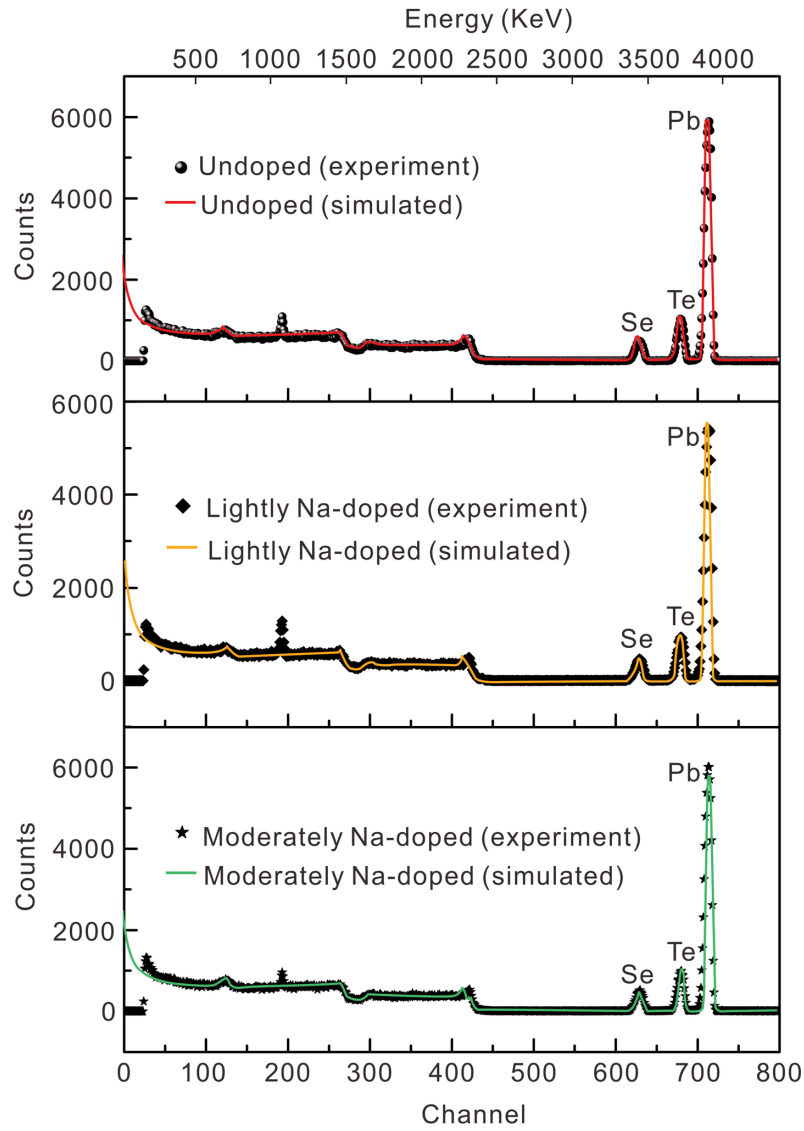


**Figure S5.** Rutherford backscattering spectroscopy (RBS) analysis of (a) undoped, (b) lightly-doped and (c) moderately-doped  $\text{PbSe}_{0.56}\text{Te}_{0.44}$  thin films on a Si substrate. The incident 4 MeV iron beam of  $\text{He}^{2+}$  was shed on the sample with a scattering angle of  $170^\circ$ . The raw data was analyzed and fitted in SIMNRA.

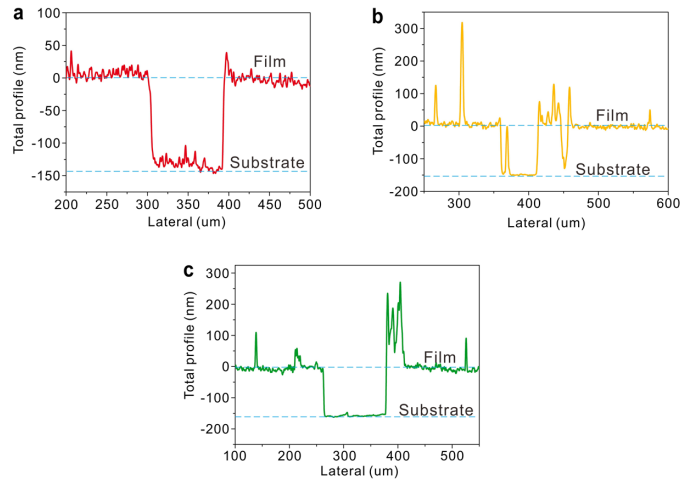


**Figure S6.** Typical profilometry curves across scratches on a) undoped, b) lightly-doped and c) moderately-doped  $\text{PbSe}_{0.56}\text{Te}_{0.44}$  thin films.

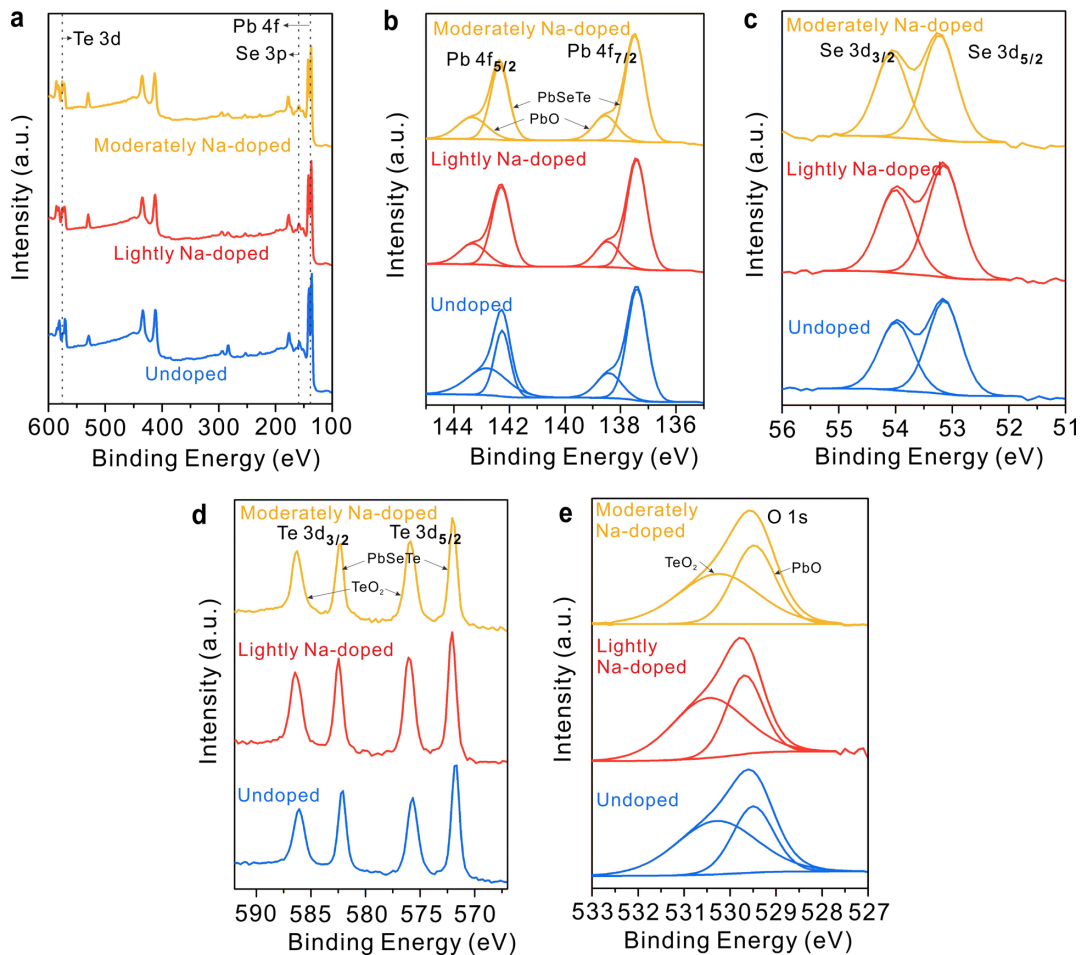


**Figure S7.** X-ray photoelectron spectroscopy (XPS) on the  $\text{PbSe}_{0.56}\text{Te}_{0.44}$  thin films before and after Na doping. (a) XPS survey spectrum of  $\text{PbSe}_{0.56}\text{Te}_{0.44}$  and Na-doped  $\text{PbSe}_{0.56}\text{Te}_{0.44}$  thin films; (b-e) XPS high resolution scan for Pb 4f, Se 3d, Te 3d and O1s regions, respectively;

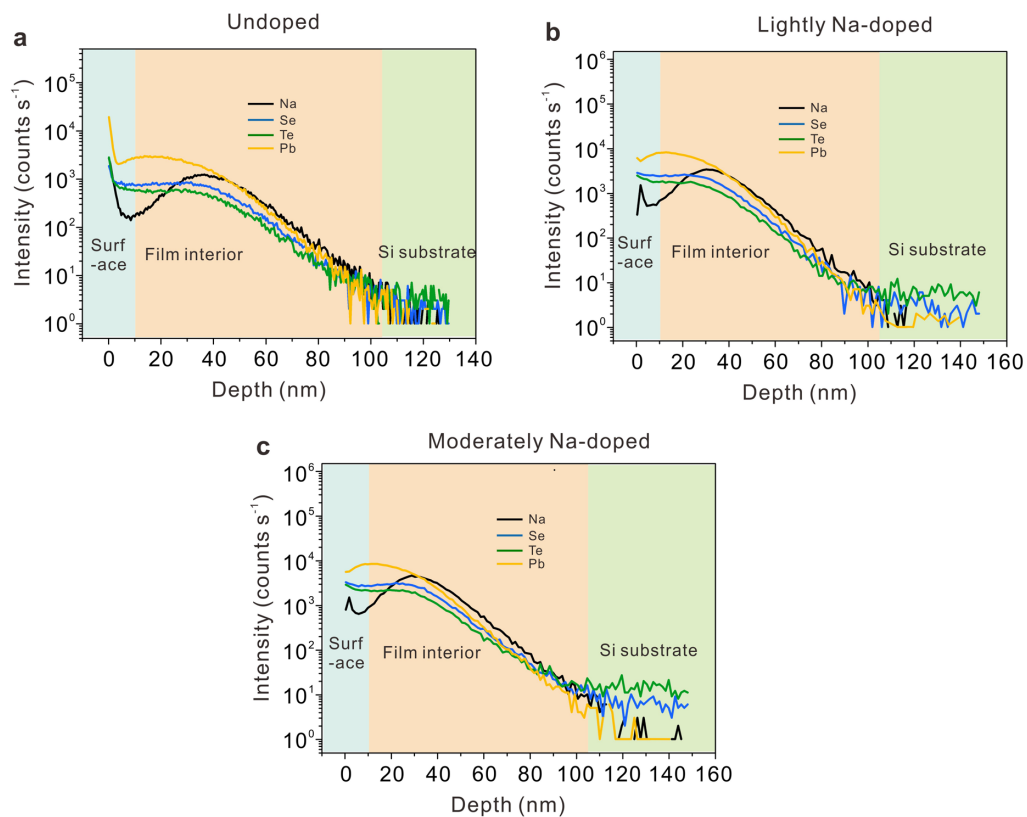
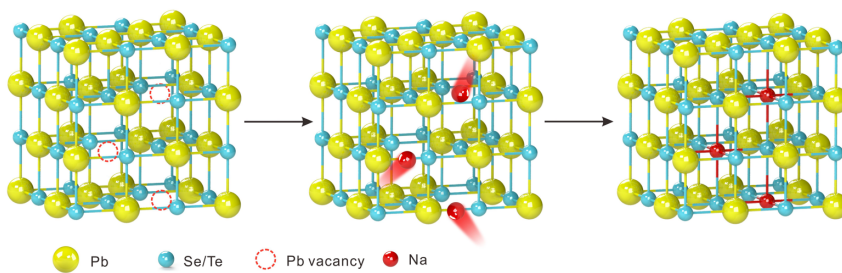


**Figure S8.** Secondary-ion mass spectroscopy (SIMS) test results of (a) undoped, (b) lightly-doped and (c) moderately-doped  $\text{PbSe}_{0.56}\text{Te}_{0.44}$  thin films deposited on Si substrates.



**Scheme S1.** The hypothesized Na doping mechanism for the  $\text{PbSe}_x\text{Te}_{1-x}$  thin films in this work.

**Table S1.** Experimental determined mass fraction (wt%) of different precursor solutions

Precursors	PbSe	PbTe	SnSe	SnTe	PbSe <sub>0.56</sub> Te <sub>0.44</sub>
Concentration (wt%)	15.8	7.8	12.8	11	12

**Table S2.** Precursor stability tests in varying environments. Although the maximum duration tested in this controlled experiment was 1 week, we note that our PbSe, SnSe, and SnTe were observed to be stable in a nitrogen environment for the duration of our entire study (i.e. months).

Environment Precursors	N <sub>2</sub> /Light	N <sub>2</sub> /No Light	Air/Light	Air/No Light
PbSe	 Stable for at least one week	 Stable for at least one week	 Precipitation happens	 Precipitation happens
PbTe	 Precipitation happens on the side wall and bottom	 Precipitation happens on the side wall and bottom	 Solidification happens at the air/liquid interface	 Solidification happens at the air/liquid interface
SnSe	 Stable for at least one week	 Stable for at least one week	 No precipitation but color change	 No precipitation but color change
SnTe	 Stable for at least one week	 Stable for at least one week	 Precipitation happens	 Precipitation happens
PbSeTe	 Precipitation happens	 Precipitation happens	 Precipitation happens	 Precipitation happens

**Table S3.** Energy-dispersive x-ray spectroscopy (EDS) test results of  $\text{PbSe}_x\text{Te}_{1-x}$  thin films prepared with varying ratios of diphenyl diselenide to diphenyl ditelluride

Ratio	Te (%)	Se (%)
1:1	45	55
1:2	63	37
2:1	33	67

**Table S4.** Thickness (nm) of  $\text{PbSe}_{0.56}\text{Te}_{0.44}$  thin films prepared via different spin-coating recipes

Spin speed (RPM) Concentration (wt%)	2500	2000	1500
12	128 ± 3	138 ± 2	150 ± 3
9.6	110 ± 3	124 ± 2	135 ± 5
7.2	70 ± 2	76 ± 3	85 ± 3
4.8	37 ± 3	50 ± 3	57 ± 3

**Table S5.** XPS binding energies comparison with literature data<sup>4-6</sup>

	Pb 4f (eV)				Se 3d (eV)		Te 3d (eV)				O 1s (eV)	
	Pb-O 4f		Pb-Se/Te 4f		Se-Pb 3d		Te-O 3d		Te-Pb 3d		O-Pb 1s	O-Te 1s
	Pb-O 4f <sub>5/2</sub>	Pb-O 4f <sub>7/2</sub>	Pb-Se/Te 4f <sub>5/2</sub>	Pb-Se/Te 4f <sub>7/2</sub>	Se-Pb 3d <sub>3/2</sub>	Se-Pb 3d <sub>5/2</sub>	Te-O 3d <sub>3/2</sub>	Te-O 3d <sub>5/2</sub>	Te-Pb 3d <sub>3/2</sub>	Te-Pb 3d <sub>5/2</sub>		
This work	143.2	138.5	142.3	137.4	54	53.3	586.2	575.8	582.5	572	529.5	530.4
Ref <sup>4</sup>			142.6	137.6	54.2	53.4	586.3	575.8	582.5	572		
Ref <sup>5</sup>	143.2	138.2	142.3	137.4	53.8	53	586.1	575.7	582.5		529.1	530
Ref <sup>6</sup>	143	138.5	142.3	137.5	54	53.1						

**Table S6.** Near surface Se/Te atomic ratio determined from x-ray photoelectron spectroscopy

Na-doping level	Se/Te
Undoped	1.34
Lightly-doped	1.42
Moderately-doped	1.61

### References

1. K. A. Borup, J. de Boor, H. Wang, F. Drymiotis, F. Gascoin, X. Shi, L. D. Chen, M. I. Fedorov, E. Muller, B. B. Iversena and G. J. Snyder, *Energ. Environ. Sci.*, 2015, **8**, 423-435.
2. L. D. Zhao, V. P. Dravid and M. G. Kanatzidis, *Energ. Environ. Sci.*, 2014, **7**, 251-268.
3. J. Q. He, L. D. Zhao, J. C. Zheng, J. W. Doak, H. J. Wu, H. Q. Wang, Y. Lee, C. Wolverton, M. G. Kanatzidis and V. P. Dravid, *J. Am. Chem. Soc.*, 2013, **135**, 4624-4627.
4. X. G. Sun, K. W. Gao, X. L. Pang, H. S. Yang and A. A. Volinsky, *J. Mater. Sci-Mater. El*, 2016, **27**, 1670-1678.
5. X. G. Sun, K. W. Gao, X. L. Pang, H. S. Yang and A. A. Volinsky, *J. Mater. Sci-Mater. El*, 2015, **26**, 7873-7881.
6. J. Song, W. Feng, Y. Ren, D. Zheng, H. Dong, R. Zhu, L. Yi and J. Hu, *Vacuum*, 2018, **155**, 1-6.